Quasiclassical Trajectory Study of $Mg(3s3p^1P_1) + H_2$ Reaction on Fitted ab Initio Surfaces

Yaw-Ren Ou, Yu-Ming Hung, and King-Chuen Lin*

Department of Chemistry, National Taiwan University, Taipei, Taiwan 106, and Institute of Atomic and Molecular Sciences, Academia Sinica, P.O. Box 23-166, Taipei, Taiwan 106, Republic of China

Received: March 3, 1999; In Final Form: August 5, 1999

Quasi-classical trajectory calculations for the reaction of $Mg(3s3p^1P_1)$ with H_2 are performed on two potential energy surfaces (PES), the excited state $^1A'$ (or $^1B_2$ in the C_{2v} symmetry) in the entrance channel and the ground state $^1A'$ (or $^1A_1$) in the exit channel. A many-body expansion procedure is adopted for the construction of the analytical fit functions from the ab initio results. The title reaction involves a nonadiabatic transition between the two potential surfaces. For simplicity, the transition probability is assumed to be unity when the trajectory goes through the region of surface crossing and changes to the lower surface. The calculated total collisional deactivation and reaction cross sections decrease with the increase of translational collision energy. The calculated rotational product distributions are characterized by a bimodal feature both for the MgH $v = 0$ and 1 states. The trend of bimodality is consistent with the observation reported in experimental studies. Our inspection of individual trajectories reveals that the low-rotational and high-rotational populations are caused by two distinct reaction pathways. This observation supports our previous expectation for the microscopic branching via the PES anisotropy. The angular product distribution indicates that the reaction proceeds predominantly via a linear collision complex. An increase of the collision energy from 2.026 to 8.104 kcal/mol has resulted in a shift of the distribution toward forward direction. The vibrational product distribution tends to decrease with the quantum numbers. The ratio of MgH($v = 1$) to MgH($v = 0$) yields a value of ~0.3, which is nevertheless underestimated as compared with the observation of 0.7 ± 0.2. The reasons for the discrepancy are also discussed.

I. Introduction

Because of the advent of state-of-the-art technologies and progress in computing accurate ab initio potential energy surfaces (PES) and performing the related scattering theories, the reaction dynamics of the first- and the second-row atoms with H_2 has continued attracting the attention of experimentalists and theoreticians. Although their reaction scheme, $A + H_2 \rightarrow AH + H$, looks as simple as $H + H_2 \rightarrow H_2 + H$, the related reaction dynamics turns out to be much more complicated than expected. For instance, the reactions $Na(4p) + H_2$[1,2] and $F + H_2$[3,4] are dominated by two distinct reaction pathways, despite the analogy of their product structures and the fact that both monohydrides meet the requirement of an octet rule. The former reaction tracks predominantly a Na-insertive, side-on attack into H_2 bond, while the latter tends to favor an H-abstraction mechanism along a collinear approach. Even among the same group of alkali atoms, the $Na(4p) + H_2$ reaction follows a pathway different from that of $K(5p) + H_2$,[5,6] in which a harpoon mechanism is invoked to account for the KH formation.

Among the reactions of alkaline earth atoms with H_2, Mg has drawn the most attention thus far. The reaction of $Mg(3s3p^1P_1)$ with H_2 has been studied for more than a decade.[7−15] Breckenridge and co-workers first found the bimodality for the rotational distributions of MgH(v=0 and 1), with the major components (~90%) peaking at very high quantum numbers and the minor components at approximately $N = 10$.[7,8] A value of 0.7 ± 0.2 was reported for the ratio of the population of $v = 1$ and $v = 0$. The reaction pathway leading to the high-N distribution was considered to originate from Mg insertion into the H_2 bond, such that one H atom release from the bent complex would induce a large torque to cause rotational excitation of the product. The pioneer finding has laid a basis for other studies with different mechanisms proposed for the low-N distribution, such as H-abstraction along an approach in collinear geometry,[7] singlet-to-triplet curve crossing,[11] decomposition directly from a linear H−Mg−H intermediate,[7,13] and collisional cooling of a rapidly rotating MgH by the free H atom which is slowly leaving from the collision complex.[7]

In an isotope effect experiment, Breckenridge and co-workers found that the nascent rotational bimodal distributions of MgH(v=0) were identical in the reaction of $Mg(3^1P_1)$ with H_2 or HD.[8] They suggested that the characteristic of bimodality should be pertinent to the exit channel dynamics on an anisotropic potential energy surface following a side-on attack of Mg insertion into H_2. Likewise, in a study on the temperature dependence, Lin and Huang observed that the MgH rotational distributions at various temperatures were coincident with each other.[12] This observation leads to a similar conclusion[8] that two distinct microscopic pathways, that occur in the exit channel, are responsible for the rotational bimodality of the nascent MgH product.

Our study of the microscopic branches for the title reaction reveals that one type of reaction pathway produces MgH in lower rotational levels and preferentially $v = 0$, while the other type produces MgH in higher rotational levels with comparable $v = 0$ and $v = 1$ populations.[13] Since the same intermediate is responsible for the two distinct rotational and vibrational distributions, the current reaction cannot be interpreted in terms of impulsive model.[16] However, by invoking the three-

* To whom correspondence should be addressed. Fax: 886-2-23621483. E-mail: kclin@mail.ch.ntu.edu.tw.

10.1021/jp9907589 CCC: $18.00
Published on Web 09/16/1999

dimensional PESs information provided by a complete active space self-consistent field (CASSCF) calculation level, one may appropriately interpret the reaction pathways involved.[14] As Mg(3^1P_1) approaches H_2 in a bent configuration along the $^1B_2$ or $^1A'$ state, the collision complex crosses nonadiabatically to the ground state and then decomposes following two microscopic pathways. In the first one, the bent intermediate, affected by a strong anisotropy of the interaction potential, decomposes via a linear HMgH geometry. The resulting MgH is anticipated to populate in the quantum states of rotational and vibrational excitation. In contrast, the second pathway produces MgH in low rotational and vibrational states, as a result of the intermediate decomposition along the stretching coordinate of the Mg−H elongation.[14]

Like the current system, discussions based on features of the PES have been widely applied in the polyatomic molecules to understand the photodissociation dynamics based on the coupling strength between the final states and the exit channel potential.[16,17] Despite the success in understanding qualitatively the internal energy distribution of the product in this manner, quantitative analysis of the measured distribution still depends on trajectory calculations. Performance of such calculations may also provide a valuable method to assess the comprehension of the current reaction mechanism by invoking the PES anisotropy.[14] For these reasons, this work is aimed to provide quantitative dynamical parameters and to propose an alternative explanation to solve the microscopic reaction pathways for the current system by performing a quasi-classical trajectory (QCT) calculation.

In this work, we have first fitted analytic potential energy functions to the ab initio three-dimensional PESs obtained previously[14] by using a many-body expansion method as suggested by Murrell and co-workers.[18,19] The QCT calculation is then performed on the fit functions of the excited state $^1A'$ (or $^1B_2$ in the C_{2v} symmetry) in the entrance channel and the ground state $^1A'$ (or $^1A_1$) in the exit channel. The calculated rotational product distributions display a feature of bimodality for the MgH $v = 0$ and 1 levels; the trend is consistent with the experimental observation. Inspection of the evolution of individual trajectories shows that the low-rotational and high-rotational populations are caused by two distinct reaction pathways. The result supports the above-mentioned interpretation of the reaction mechanism by invoking the PESs anisotropy.[14] Nevertheless, the population ratio of MgH(v=1) to MgH(v=0) is underestimated, as compared with the experimental finding.[7] The reasons for the discrepancy will be discussed. In the present study, we also explore the behavior of other results from the calculation including opacity function, total collisional deactivation and reaction cross sections, and angular product distribution.

II. Computation Processes

A. Analytical Potential Energy Function. The ab initio PESs with the CASSCF calculation level obtained previously[14] for the excited ($^1A'$ or $^1B_2$) and the ground states ($^1A'$ or $^1A_1$) in the $Mg(3^1P_1) + H_2$ reaction have been fitted to the analytical expression through the adoption of the many-body expansion function suggested by Sorbie and Murrell.[18] The function contains three two-body terms and one three-body term, i.e.,

$$V(R_1,R_2,R_3) = V^{(2)}{}_{MgH}(R_1) + V^{(2)}{}_{MgH}(R_2) + V^{(2)}{}_{HH}(R_3) + V^{(3)}(R_1,R_2,R_3) \quad (1)$$

where R_1 and R_2 are the two MgH distances and R_3 is the HH separation. The analytical function expressed in eq 1 is valid for the ground state but must include an additional one-body term, $V^{(1)}{}_{Mg} = 4.6908$ eV, for the description of excited state. The MgH diatomic potentials are represented by an extended Rydberg function,[18,19]

$$V^{(2)} = -D_e(1 + a_1\rho + a_2\rho^2 + a_3\rho^3)\exp(-a_1\rho), \quad \rho = R - R^\circ \quad (2)$$

which has a minimum at the equilibrium distance, i.e., $\rho = 0$ ($R = R^\circ$). Dunham has derived expressions for the rotation−vibration energy levels of a diatomic molecule in terms of derivatives of the potential at the equilibrium distance.[18,20] The second, third, and fourth derivatives of the potential at $\rho = 0$, denoted as f_2, f_3, and f_4, respectively, may be expressed by the related spectroscopic parameters. The coefficients a_1, a_2, and a_3 are then obtained by solving a set of coupled equations containing these derivatives of the potential. The Dunham expansion parameters and the derivatives of potentials in the system are given in Table 1.

TABLE 1: Dunham Expansion Parameters[a] and Force Constants for H_2, MgH($X^2\Sigma^+$), and MgH($A^2\Pi$)

parameter	H_2	MgH($X^2\Sigma^+$)	MgH($A^2\Pi$)
R_e/Å	0.7414	1.7297	1.6778
w_e/cm^{-1}	4401.213	1495.20	1599.50
w_ex_e/cm^{-1}	121.336	31.889	32.536
w_ey_e/cm^{-1}	0.8129	0.384	−0.146
B_e/cm^{-1}	60.8530	5.8257	6.1913
α_e/cm^{-1}	3.0622	0.1859	0.1931
f_2/aJÅ^{-2} [b]	5.751	1.27436	1.455923
f_3/aJÅ^{-3} [b]	−37.4	−5.227	−6.09636
f_4/aJÅ^{-4} [b]	238	17.0833	21.7748

[a] See ref 31. [b] aJ = mdyne Å.

The three-body term $V^{(3)}$ can be expressed by the product of a polynomial, $P(R_i)$, and a range function, $T(R_i)$, as follows:[18,19]

$$V^{(3)}(R_1,R_2,R_3) = P(R_i)\,T(R_i) \quad (3)$$

$$P(R_i) = V^\circ(1 + \sum_i C_i\rho_i + \sum_{i\le j} C_{ij}\rho_i\rho_j + ...); \quad \rho_i = R_i - R_i^\circ \quad (4)$$

$$T(R_i) = (1 - \tanh\gamma_1 S_1/2)(1 - \tanh\gamma_3 S_3/2) \quad (5)$$

where

$$S_1 = \sqrt{1/2}(R_1 + R_2 - R_1^\circ - R_2^\circ) \quad (6)$$

$$S_3 = R_3 - R_3^\circ \quad (7)$$

In such an expression, the three-body term tends to zero if one atom in the triatomic system is removed to infinity. Here P is a polynomial of up to the fourth order in the three internuclear distances; T is expressed in terms of symmetry coordinates. There are 26 parameters contained in the three-body term both for the excited and the ground state. The optimization of these parameters including V^o, R_1(MgH), R_3(HH), γ_1(MgH), γ_3(HH), and 21 coefficients in P was achieved by least-squares fit to the 400 ab initio points each on the excited and the ground potential surface.

Table 2 presents the parameters of the fit functions. An example of two-dimensional PESs for the excited ($^1B_2$) and the ground state ($^1A_1$) generated with these parameters is shown in Figure 1. The obtained χ^2, which is indicative of the deviation from the ab initio energy, is 0.38 for the excited state and 0.58

TABLE 2: Parameters of the Potential Functions of MgH_2[a]

One-Body Term
$V_{mg}^{(1)} = 4.6908$ eV

Two-Body Terms

species	D_e/eV	R_e/Å	a_1/Å^{-1}	a_2/Å^{-2}	a_3/Å^{-3}
MgH($X^2\Sigma^+$)	1.33	1.7297	4.0884	5.3667	3.2515
MgH($A^2\Pi$)	1.6136	1.6778	3.892	4.755	2.793
H_2	4.7472	0.7414	3.961	4.064	3.574

Three-Body Terms

parameter	excited state	ground state
V^0/eV	−0.89936	3.90464
R_1^0(MgH)/Å	1.8853	2.0485
R_3^0(HH)	1.6863	1.26604
γ_1(MgH)/Å^{-1}	0.54676	0.87045
γ_3(HH)	0.76725	0.68400
C_1/Å	1.3674	0.05389
C_3	3.43743	0.01581
C_{11}/Å^{-2}	−1.54953	−0.20377
C_{33}	−1.26911	−0.6152
C_{12}	2.3134	0.49170
C_{13}	−1.0573	0.84511
C_{111}/Å^{-3}	−0.72686	0.16940
C_{333}	−0.49385	0.29286
C_{112}	1.41288	−0.27309
C_{113}	1.24457	−0.19728
C_{133}	2.08732	−0.44373
C_{123}	−1.22768	−0.98922
C_{1111}/Å^{-4}	0.68452	0.09413
C_{3333}	0.25904	−0.05605
C_{1112}	−1.70146	−0.19113
C_{1122}	1.01021	0.23733
C_{1113}	−0.52373	0.03974
C_{1133}	−0.88338	0.17083
C_{1333}	−0.64148	−0.32589
C_{1123}	1.49659	0.07683
C_{1233}	0.73156	0.25425

[a] The two-body terms are extended Rydberg functions, and the three-body terms are the product of a polynomial and a range function. By symmetry $C_1 = C_2$, etc.

for the ground state. The maximum deviation from the ab initio energy is 1.5 kcal/mol for the excited state of HMgH at a bond angle of 12° and 2.0 kcal/mol for the ground state at 60°. Both maximum errors occur at a rather high point on the repulsive regions and hence are not expected to have significant influence on the QCT results.

As shown in Figure 1a, the potential energy tends to decrease with decreasing the Mg− H_2 distance along the $^1B_2$ surface. The H_2 bond has to elongate before the collision complex reaches the crossing region, where there exists a minimum energy at the position of $R_2 = \sim 1.8$ Å and $R_1 = \sim 1.4$ Å. After going through the crossing seam, the bent-shape collision complex in the ground state surface with higher energy becomes unstable and may break apart predominantly along two low-energy directions as shown in Figure 1b. When R_2 is shortened and R_1 is elongated, MgH + H can be formed. In contrast, as R_1 is moved close to the H_2 equilibrium distance and R_2 is lengthened, Mg(3^1P_1) + H_2 may proceed physical quenching to yield Mg(3^1S_0) + H_2. As reported previously, if the ground state PES is plotted as a function of Mg−H distance and bending angle, with the other MgH fixed at the equilibrium position, the feature of MgH_2 complex dissociation in the reaction channel becomes more recognizable.[14] The plot shows that the potential energy tends to decrease along two directions; one is the Mg−H elongation, and the other is the angle expansion. When the bending angle is increased to 180°, the potential surface falls down to the well, 3.8 eV below that of the Mg(3^1P_1) + H_2 reactants.[14] The MgH_2 complex is expected to break apart following these two microscopic pathways.

The fit functions have been adopted to regenerate the related potential surfaces for the C_{2v} or C_s geometries of Mg + H_2. Each analytical potential function is fitted to 400 ab initio points, which are calculated for varied geometries of Mg + H_2 in either C_s or C_{2v} symmetry nearby or at the crossing region. The ab initio diabatic potential surfaces in C_{2v} symmetry is readily computed, but the PESs calculations may become difficult to converge, when Mg + H_2 in C_s geometry comes close to the crossing region.[14] To optimize the fit parameters, we have compared the fitting energies with these ab initio values. The obtained analytical potential functions determine the crossing seam (Figure 1), within which the fit potential energy of the ground state is higher than that of the excited state. The case of collinear approach is omitted for the reason that the collision following either $^1\Pi$ or $2^1\Sigma^+$ PESs in the $C_{\infty v}$ approach may encounter an energy barrier as high as 1.67−1.8 or 1.36−1.7 eV, respectively.[11,14] The H abstraction reaction in a collinear attack is therefore very difficult.

B. Qusiclassical Trajectory Calculation. A classical trajectory program by Chapman et al. was utilized for the scattering calculations in this work.[21] The current reaction involves a nonadiabatic surface crossing, and there are various sophisticated methods to evaluate the transition probability. But in this work the transition probability is assumed to be unity, when the trajectories go through the crossing region and change to the lower surface. Such a surface transition takes place according to the following rule. The trajectories initially evolve on the excited state surface prior to the surface crossing and after the first entry into the crossing region. The first entry is encountered when the potential energy of the ground state begins to exceed that of the excited state. Then, the trajectories switch instantaneously onto the ground-state surface at the second crossing entry, where the potential energy difference is reversed. Here, the case of multiple entries (more than two entries) is neglected since the probability for such crossings should be very small. It is also noted that the system is treated as a single-surface analogue. No energy gap exists between excited and ground state surfaces at the crossing seam. As long as the trajectory evolves with a very small step, the final velocity of the collision complex prior to the second crossing entry may be considered as its initial velocity while jumping onto the ground state surface. In this manner, the angular momentum may be conserved.

For our trajectory calculations, the following data and conditions are adopted. The initial collision energy ranges from 2.026 to 8.104 kcal/mol, corresponding to a reaction temperature from 800 to 3200 K based on the Boltzmann law. For simplicity, the initial H_2 energy is kept in the quantum state of $(v,j) = (0,0)$, although the nonzero rotational levels may be populated. The other initial conditions including impact parameter, azimuthal and polar orientation angles of H_2 internuclear axis, orientation of H_2 angular momentum, and phase angle of H_2 vibration are sampled with a random number generator. The trajectories are initiated at a Mg−H_2 internuclear separation of 3.4 Å and evolved at a step of 1×10^{-17} s to achieve energy conservation up to at least five figures. The back integration of trajectories to recover the initial conditions is not checked in this work. Thus, the accuracy of trajectory may sometimes be less than the significant figures conserved for the total energy.[22] A total number of 1200 trajectories are run for each initial collision energy. When a trajectory computation is completed, the way of slicing up the continuous distribution of final vibrational and rotational energies contained in MgH into

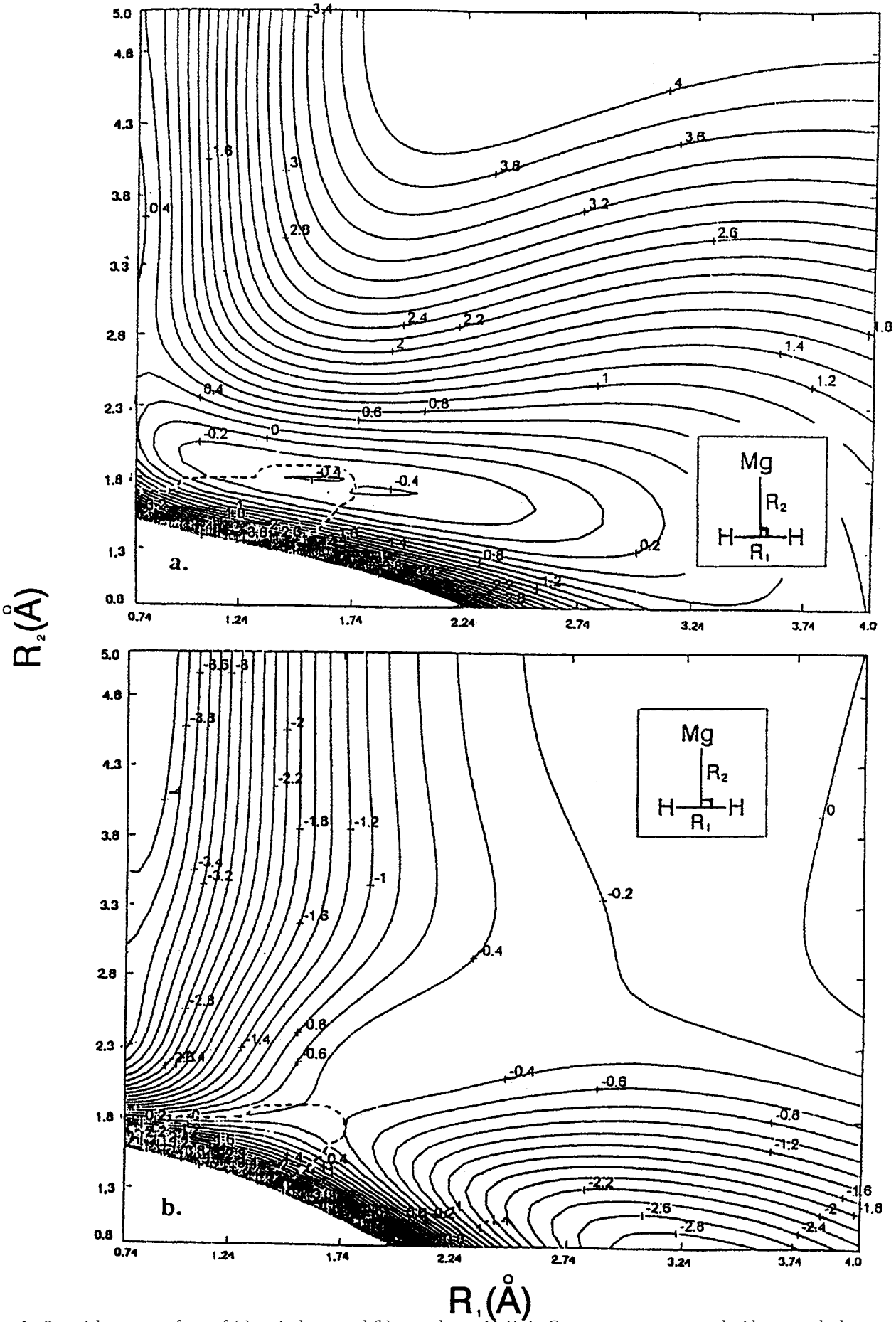

Figure 1. Potential energy surfaces of (a) excited state and (b) ground state MgH_2 in C_{2v} geometry, as generated with a many-body expansion function, respectively. The dashed curves indicate the surface crossing seams.

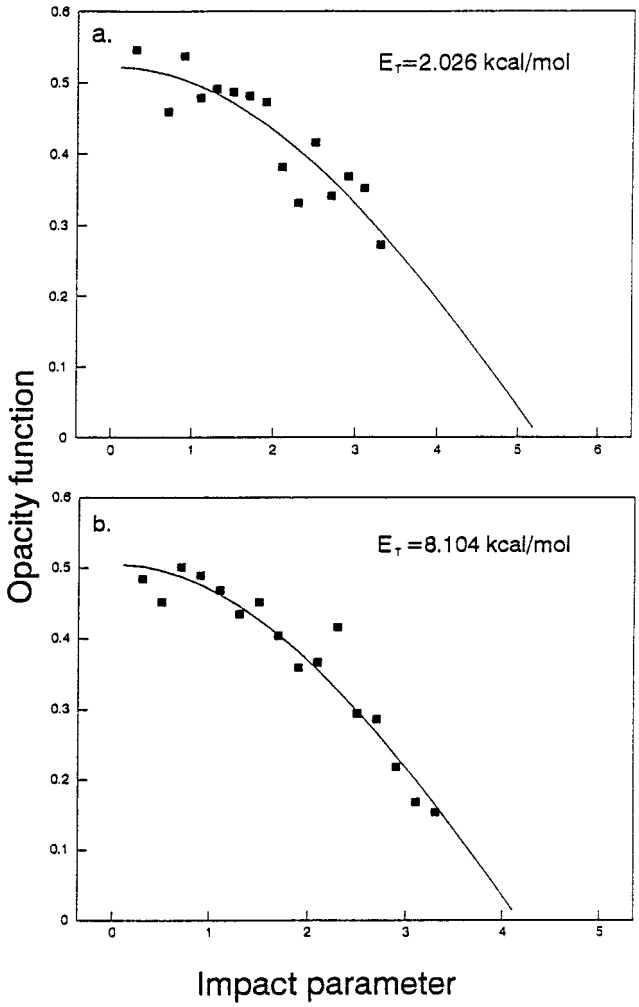

Figure 2. Collision energy dependence of the opacity function for the reaction. Collision energies are (a) 2.026 and (b) 8.104 kcal/mol. The initial interatomic separation of Mg−H_2 is 3.4 Å. The solid line indicates the least-squares fit based on eq 9 in the text. The square symbol denotes the results from QCT calculations.

quantum state (v, N) obeys the following rule. If the obtained classical energies are within the halfway of the quantized energy gaps from a closest quantum state, then the portion of energy is assigned to this particular state.[23]

III. Results and Discussion

A. Total Reaction and Collisional Deactivation Cross Sections. Figure 2 shows two plots of opacity functions, i.e., reaction probabilities, versus impact parameter for the two collision energies of 2.026 and 8.104 kcal/mol. On the basis of trajectory calculations, the opacity function for chemical reaction is defined as

$$P(E,b) = Nr(E,b)/N_T(E,b) \tag{8}$$

where $Nr(E,b)$ is the number of reactive trajectories at energy E in the impact parameter between intervals [b, b + db]; N_T-(E,b) is the total number of such trajectories. In this work, the following analytical function is used to approximate the opacity function $P(b)$:[24]

$$P(b) = a\cos(\pi b/2b_{max}) \tag{9}$$

The parameters a and b_{max} have been optimized from a least-squares fit. The obtained b_{max} is used as the upper limit of the impact parameter, and the intervals of $0 \le b \le b_{max}$ are randomly generated, as mentioned in section II.B, to perform the trajectory calculations. If b is fixed at the value of b_{max}, the obtained reaction probability is almost zero as a result of 1200 trajectory computation, consistent with that determined by eq 9. The reaction cross section is therefore calculated by

$$\sigma = 2\pi\int_0^{b_{max}} P(b)b\,db \tag{10}$$

TABLE 3: Parameters a and b_{max} of Opacity Functions, Total Collisional Deactivation, and Reaction Cross Sections[a]

collision energy (kcal/mol)	a	b_{max}	cross section (Å^{-2})
0.507	0.52 (0.56)	6.27 (8.58)	29.70 (60.31)
2.026	0.53 (0.60)	5.05 (6.42)	19.67 (33.05)
4.052	0.57 (0.64)	4.35 (5.00)	15.61 (23.42)
8.104	0.54 (0.68)	4.00 (4.40)	12.65 (19.22)
12.156	b (b)	b (b)	8.90[c] (b)
16.208	b (b)	b (b)	7.28[c] (10.23)[c]

[a] The values without the parentheses are the reaction cross sections; the values in the parentheses are collisional deactivation cross sections. [b] Uncalculated. [c] Calculation by the approximation method, $\sigma = 2\pi\int_0^{bm} dbP(b)b \approx 2\pi\sum_{b=0}^{bm} b\,P(b)\Delta b$; $\Delta b = 0.2$.

The resulting parameters and the reaction cross sections at various collision energies are exhibited in Table 3 and also displayed in Figure 3. The shapes of opacity functions are characteristic of two features. First, the opacity function tends to monotonically decrease to zero at b_{max}, within which the reaction may occur. The overall similarity of the shapes for the collision energies studied indicates that the rotation of H_2 has little effect on the reorientation of the initially unfavorable MgHH configuration toward more favorable dispositions, as the approaching time between Mg and H_2 is varied. It should be noted that the initial interatomic separation between Mg and H_2 is smaller than the b_{max} value, as is constrained by the accuracy of fit functions of PESs. The fitting reliability becomes poor as the approaching distance is larger than 3.8 Å. Nevertheless, the shortcoming seems to be tolerable in the prediction of the cross sections studied and the rotational product distribution. Second, the b_{max} values decrease as the collision energies increase. This tendency is typical for the reaction in which a transitory complex is formed by the attractive interaction. With increase of the initial relative velocity, the lifetime of the collision complex is shortened. Therefore, decomposition of the energetic complex cannot be effectively channeled into the reactive products. By analogy with this work, the reaction of $O(^1D) + H_2$ proceeds via an energetic H_2O complex as intermediate following an attractive insertion mechanism.[25] The corresponding b_{max} value as a function of collision energy shows a similar trend as in this work. In contrast, for the reaction of $N(^4S_u) + NO \rightarrow N_2 + O$, the domination of a direct mechanism leads to backward scattering, despite the absence of energy threshold in the way.[26] In this case, the b_{max} value, equal to a small collision diameter of 2.5−2.7 Å, is independent of the collision energies.

As shown in Figure 3, the resultant reaction cross sections, evaluated by eq 10, decrease with increasing translational collision energy in the range from 0.5 to 16 kcal/mol. This fact implies that an attractive force should act on the collision of Mg and H_2, in accordance with the characteristic of an insertion mechanism reported previously. Such a behavior may arise from the less efficiency of energy transfer from the collision complex into product channels with increase of the kinetic energy, as described above.[27]

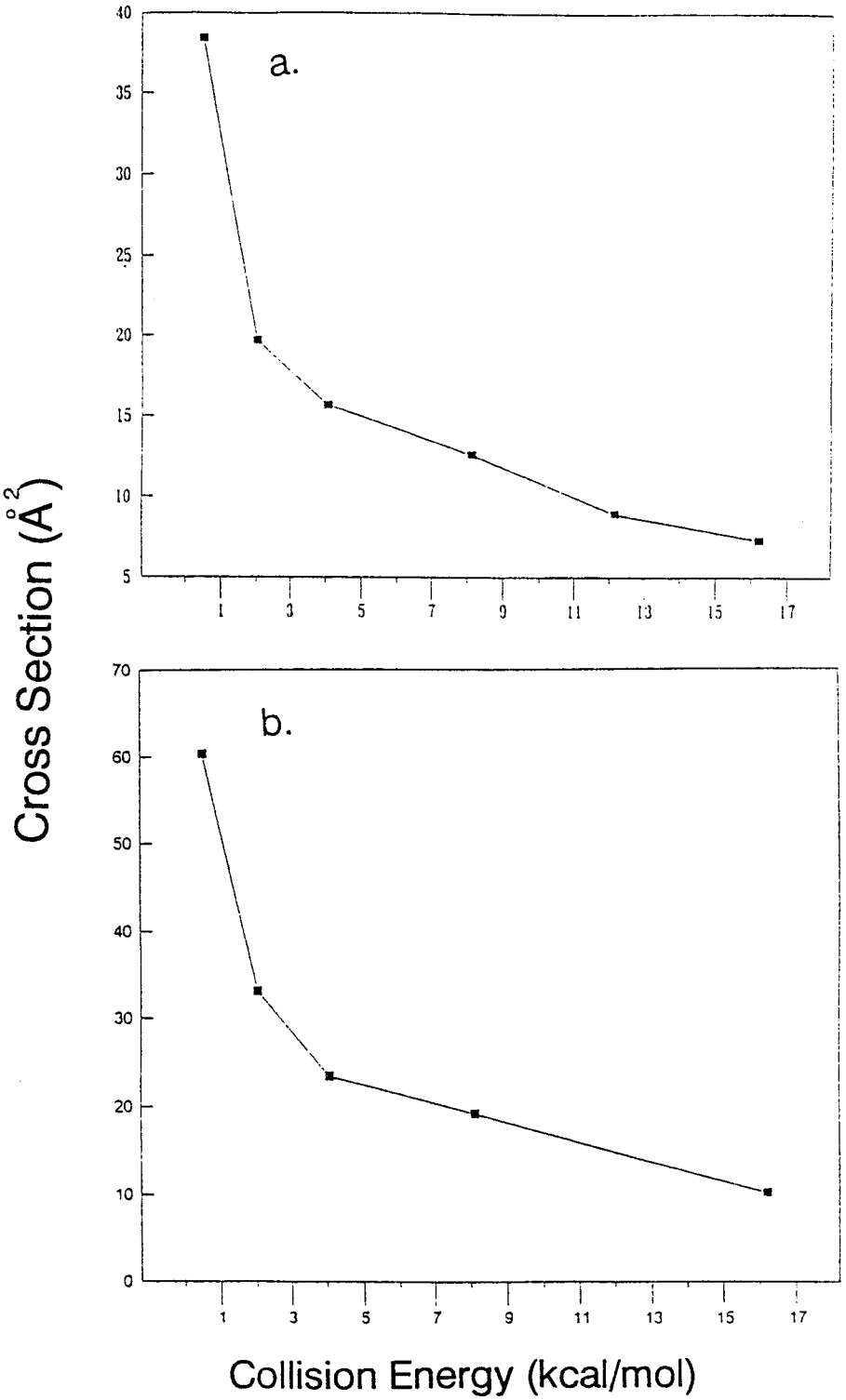

Figure 3. Collision energy dependence of (a) reaction cross section and (b) total collisional deactivation cross section.

In this work, we have also evaluated the total collisional deactivation cross sections as a function of the collision energy, by determining the corresponding opacity function as a ratio of the trajectories going through the surface crossing to the total number of trajectories. The kinetic energy dependence in Figure 3b appears to have similar behavior as the reaction cross section. The total collisional deactivation cross section takes into account the disappearance of $Mg(3^1P_1)$ in the presence of H_2. That is, the trajectories, which do not go through the crossing region and re-form the $Mg(3^1P_1) + H_2$ reactants, do not contribute to the quenching process. After transition to the lower PES, there open two quenching channels: $MgH + H$ and $Mg(3^1S_0) + H_2$. The former products may contribute to the reaction cross section, while the sum of these two quenching channels contributes to the total collisional deactivation cross section. Note that the total collisional deactivation cross section obtained at 1.3 kcal/mol, interpolated from Figure 3b, is about 50 Å^2, which is larger than the experimental observation of 31.4 ± 0.8 Å^2 by Breckenridge and Umemoto in a bulb condition at 426 K (equivalent to 1.3 kcal/mol).[28] This may be attributed to the neglect of the other two degenerate states of $^1A_1$ and $^1B_1$ (in C_{2v} symmetry) in our trajectory computation, such that the

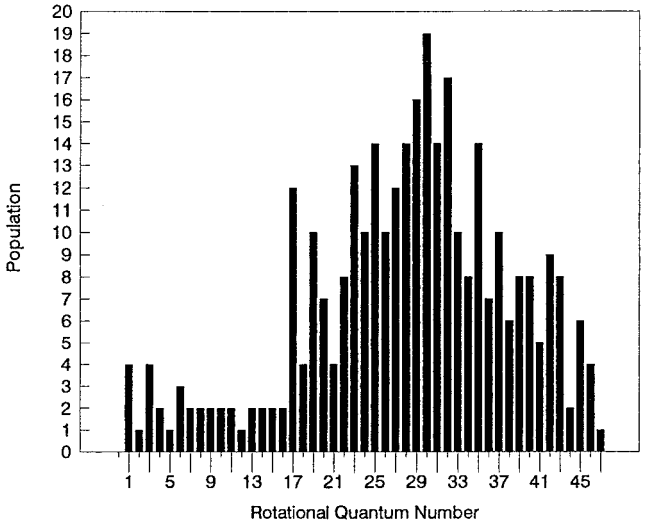

Figure 4. Roational population distribution of MgH(v=0) resulting from the QCT calculation.

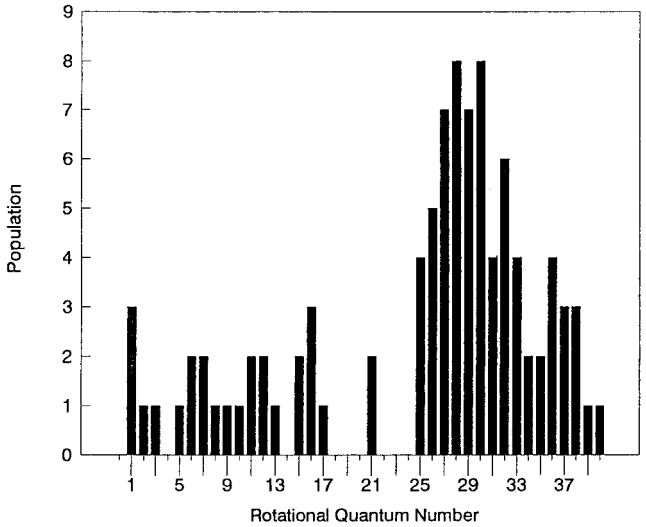

Figure 5. Roational population distribution of MgH(v=1) resulting from the QCT calculation.

number of trajectories going through the crossing region is overestimated. In fact, the behavior of collisional quenching is more complicated than that confined by this work. When inspecting parts a and b of Figure 3, one may find that the probability for a reaction varies from ~63% at low energies to ~70% at high energies, after transition to the lower PES.

B. Rotational Population Distribution. From the QCT calculations, rotational populations of MgH have also been obtained. Figures 4 and 5 show some typical results for $v = 0$ and $v = 1$, calculated respectively at the energy of 2.026 kcal/mol. The population is represented by the number of reactive trajectories. Since only 1200 trajectories are calculated, the contributions to specific states are rather small. For example, only 19 trajectories occur at the peak of the high rotational component of MgH(v=0). Despite the limited number of trajectories, the shapes of the distributions generally exhibit a bimodal feature for both MgH $v = 0$ and 1, with a dominant high-N component and a minor low-N component. For $v = 1$, the populated rotational quantum states are limited by N(max) = 40 at the expense of vibrational excitation. One should note that the limited number of trajectories may not sample over all of the phase space in the reaction channel. However, we have calculated respectively both 500 and 1000 trajectories and found that the resulting peak positions are similar to that obtained from 1200 trajectories and the low-N component still appears even for 500 trajectories. The bimodal feature of the calculated rotational distribution fits qualitatively to the observation at 750−760 K (Figures 4 and 5).[13] The increase of the number of trajectories should certainly improve the quality of the rotational distribution.

As mentioned previously, the microscopic branching pertinent to the rotational product distribution may be caused by the anisotropy of the interaction potential in the exit channel.[14] The two-dimensional PESs(d, θ), either calculated by the ab initio level or regenerated by its fit function, show two reaction pathways along which the collision complex may break into the final products. One is to elongate the stretching direction of the Mg−H bond to render the MgH product in the levels of low rotation and low vibration; the other track goes through the linear HMgH geometry before decomposing, and thereby MgH is produced in the rotational and vibrational excitation.

To understand such a microscopic branching, we analyze the representative sampling of trajectories pertinent to the low-N and high-N MgH(v=0 and 1) products at the collision energy of 2.026 kcal/mol. Inspecting the examples of the individual trajectories selected in Figures 6 and 7, we find that the reactive times for both low-N and high-N trajectories are short within the 10^{-13} s range. Here, some uncertainties are inevitable for the reason that the fitting quality of the analytical function becomes poor at the Mg−H_2 separation beyond 3.8 Å, and therefore, we stop our calculations at H−H distances of 5−6 Å. According to Figures 6 and 7, marked difference between low-N and high-N trajectories may be found in the geometry of collision complex in the exit channel and the corresponding potential energy carried. For the low-N trajectories ($N = 3$, $v = 1$), one H atom from the MgH_2 complex is removed along a direction in which the bending angle of H−Mg−H is enlarged to some extent before dissociating (Figure 6a). The MgH_2 complex is subject to a weak anisotropic coupling between the stretching coordinate and the bending angle. This fact satisfies the proposed pathway based on the PESs information, but opens up more avenues to form the low-N product. Elongating the Mg−H bond alone is not the only pathway. In contrast, for the high-N trajectories ($N = 33$, $v = 0$), the dissociative complexes are almost in a linear geometry, having the bending angles of HMgH at about 180° in the exit channel (Figure 7a). This type of collision complex is exposed to a strong anisotropic interaction of the exit channel potential, as expected by the PES information.[14]

Figures 6 and 7 also show the potential energies corresponding to specific interatomic distances in the trajectories analyzed. For the low-N trajectory ($N = 3$, $v = 1$), the potential energy carried in the dissociative complex changes slightly with the reactive time after transition to the lower state (Figure 6b). The complex with little energy carried may accordingly lead to the final products in the quantum states of low rotation. In contrast, for the high-N trajectory ($N = 33$, $v = 0$), the potential energy carried in the dissociative complex changes dramatically after transition to the lower state (Figure 7b). The complex with such large amount of energy may cause the final products in the rotational excitation. To test reliability of the representative sampling of trajectories, we have also examined the trajectories leading to MgH($N = 7$, $v = 0$) and ($N = 25$, $v = 1$) and obtained similar results as shown in Figures 6 and 7.

A drawback for the above trajectory calculations is that they are terminated at a short interatomic separation, which provides little information about the end result. To gain an insight in the

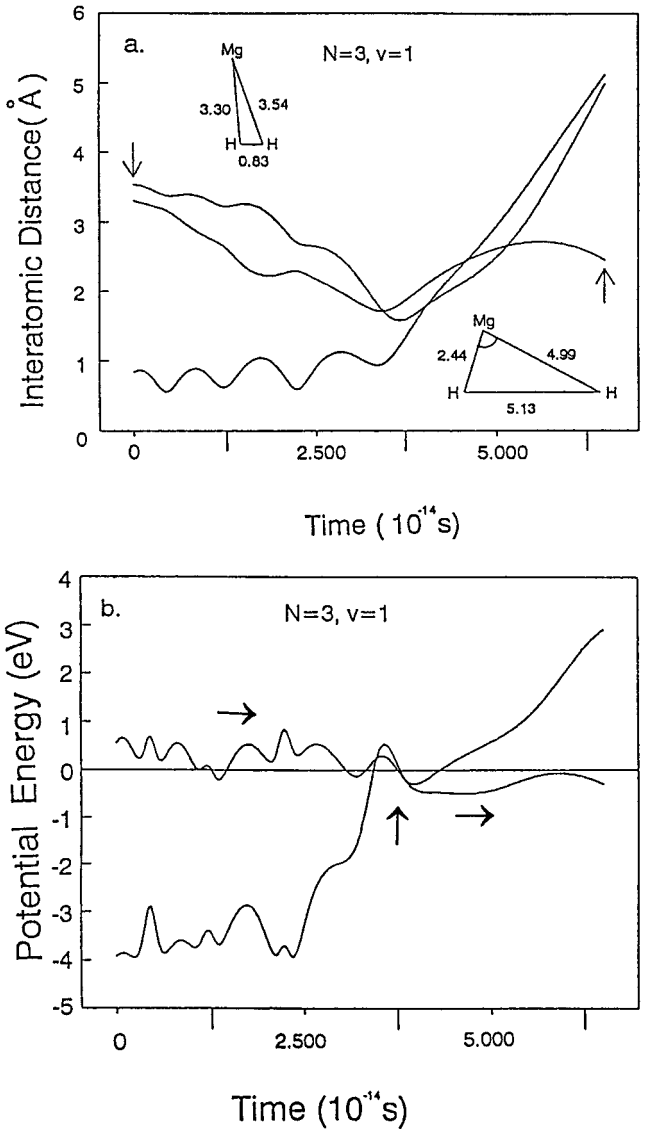

Figure 6. (a) Evolution of trajectory for the low rotational level of MgH at $N = 3$ ($v = 1$). (b) Interaction potential for a specific interatomic separation in the trajectory for the low rotational level at $N = 3$ ($v = 1$). Arrow (→) indicates the direction of trajectory, and arrow (↑) denotes the entry for trajectory jumping to the lower surface.

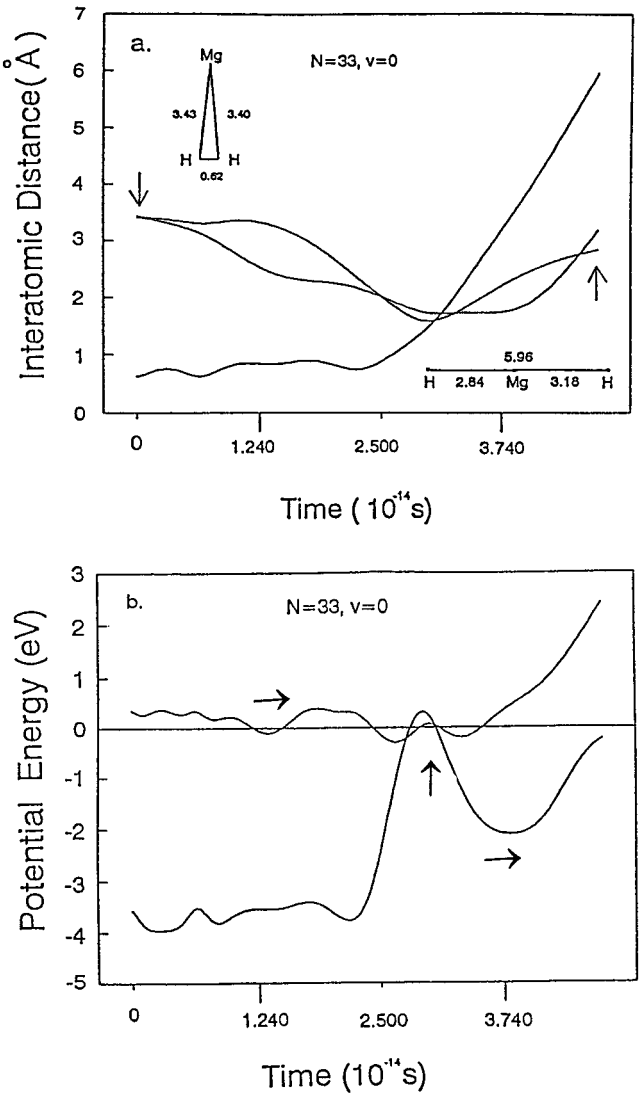

Figure 7. (a) Evolution of trajectory for the high rotational level of MgH at $N = 33$ ($v = 0$). (b) Interaction potential for a specific interatomic separation in the trajectory for the high rotational level at $N = 33$ ($v = 0$). Arrow (→) indicates the direction of trajectory, and arrow (↑) denotes the entry for trajectory jumping to the lower surface.

exit channel, we let the trajectories to go on beyond the fit potential function. Figure 8 shows such trajectories leading to the rotational levels of $N = 4$ and $N = 31$ in MgH(v=0) at initial kinetic energy of 2.026 kcal/mol. These two types of trajectories are found to differ in three aspects. First, for the high-N trajectory, the collision complex reaches a linear geometry rapidly ($<5 \times 10^{-14}$s) within a short bond distance between H and Mg (~2 Å). In contrast, for the low-N trajectory, the collision complex reaches the same linear geometry slowly ($>1.1 \times 10^{-13}$ s). In addition, the departing H atom is far away from the Mg atom (~8 Å), because of weak coupling between the radial and angular parts of the ground state potential surface. The phenomenon demonstrates that the high rotational distribution is caused by a strong PES anisotropy, while the low rotational distribution is subject to a weak PES anisotropy. This is consistent with the results described above.

Second, the collision complex for the high-N component is much more long-lived than that for the low-N component. As shown in Figure 8, the former complex lingers for some time in a linear geometry before dissociating, but the latter one breaks apart rapidly without changing much of its geometry. The phenomenon, which has also been found by Sando and Hung,[29] however, becomes unclear when the trajectories are terminated earlier. Third, once the H atom departs from the high-N collision complex, it gains a larger speed than that leaving from the low-N collision complex. This may be verified by comparing the distances between leaving H and Mg at the same dissociating times. One possible explanation is that the high-N collision complex is subject to a strong attractive interaction and the depth of the potential well for the linear complex is about 3.8 eV below the reactants.

Breckenridge and Wang have performed half-collision classical trajectories calculation on a model PES of triatomic molecule HMH (or HMD) in which a rigid rotor of MH product is assumed.[30] In their study, the leaving H (or D) isotopic effect depends significantly on the anisotropy parameter, which is indicative of the coupling strength between radial and angular parts of the potential. They have found that, as the anisotropy parameter increases, the leaving H (or D) of the HMH (or HMD) complex tends to accelerate the angular motion at a decreased distance of H−M (or D−M) bond. The dependence of individual trajectories on the PES anisotropy shows a tendency similar to

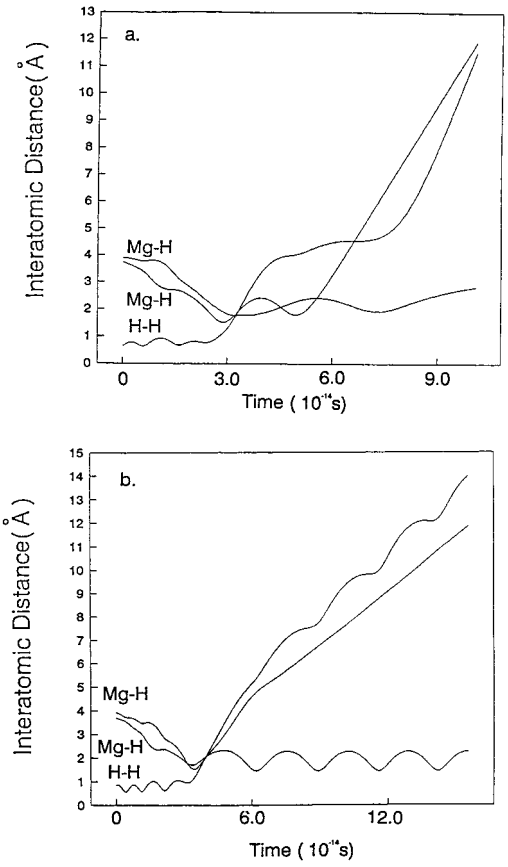

Figure 8. Evolution of trajectories for the rotational levels of MgH at (a) $N = 31$, $v = 0$ and (b) $N = 4$, $v = 0$. Initial kinetic energy is fixed at 2.026 kcal/mol.

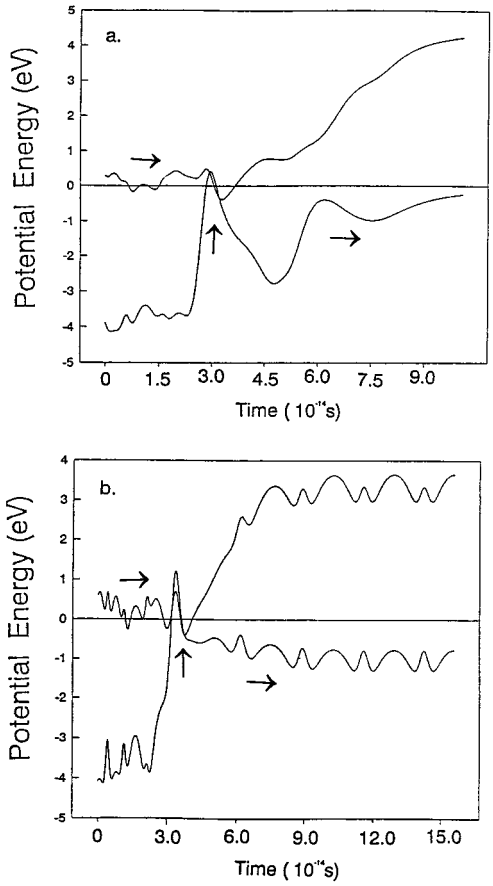

Figure 9. Interaction potential for a specific interatomic separation in the trajectories for the rotational levels of MgH at (a) $N = 31$, $v = 0$ and (b) $N = 4$, $v = 0$. Initial kinetic energy is fixed at 2.026 kcal/mol. Arrow (→) indicates the direction of trajectory, and arrow (↑) denotes the entry for trajectory jumping to the lower surface.

our results described above. When applying the trajectory calculation to the HMgH system, the authors have suggested that the low-N component of the MgH rotational bimodality may be caused by a less anisotropic portion of the same singlet potential surface. The suggestion is also consistent with our conclusion of trajectory computation.

For the low-N and high-N trajectories, the potential energy states corresponding to individual geometries of collision complex along the reaction coordinate are shown in Figure 9. In Figure 9a, the high-N collision complex, after transition to the lower state, still carries a large amount of internal energy and then oscillates to dissipation along the dissociating coordinate. In contrast, the collision complex forming the low-N component, with small internal energy, reaches equilibrium rapidly (Figure 9b). This feature is closely related to the anisotropic interaction of the exit channel PES. Because of the strong anisotropic interaction in the formation of high-N MgH, the MgH_2 complex changes dramatically in geometry from a bent to a linear shape within a short bond distance of H−Mg; the subsequent energy change therefore becomes huge.

In general, the trajectories shown in Figures 8 and 9 provide similar information as in Figures 6 and 7, but may be more conclusive. However, one should note that in the current study the shortcomings involved in the entrance and the exit channels might cause some undiscernible impact on the outcome. In contrast to the exit channel trajectories, it is difficult to find significant difference between low-N and high-N distribution in the entrance channel trajectories, concerning the initial collisional geometry, the shape of the collision complex, and entry to the crossing region.

C. Vibrational Population Distribution. Using a pump−probe technique in a bulb system, Breckenridge and co-workers have found the MgH product with the vibrational population up to 2.[7] The reported ratio 0.7 ± 0.2 for MgH(v=1)/MgH(v=0) is in accordance with a value of 0.8 from our previous result.[13] The current trajectory calculation yields a vibrational population distribution in Figure 10, showing a monotonic decrease with the quantum numbers. The distribution thus obtained displays the same trend as in the experiment. However, the resulting MgH(v=1)/MgH(v=0) value of ∼0.3 is underestimated. The reasons to cause the discrepancy are yet to be known. It may be attributed to incomplete energy redistribution in the final products. As restricted by the scope of ab initio PESs provided,[14] the internuclear separation is not far enough before the trajectory calculation is terminated.

D. Angular Distribution in Products. The angular distribution of MgH in the center-of-mass framework is obtained by estimating the number of reactive trajectories with the product scattered in an interval of 10° out of the total trajectories scattered in such an interval. The result is shown in Figure 11. Note that the obtained angular distribution of MgH is related to the differential cross section multiplied by sin θ; θ is the scattering angle. Therefore, the resultant scattering distribution for the collision energy of 2.026 kcal/mol is nearly forward−backward symmetric, but with a slight forward bias. The slight asymmetry in the scattering distribution may suggest that the reaction proceeds predominantly via a linear collision complex in the exit channel. The energized linear intermediate with a state energy of 3.8 eV below the $Mg(3^1P_1) + H_2$ reactants is

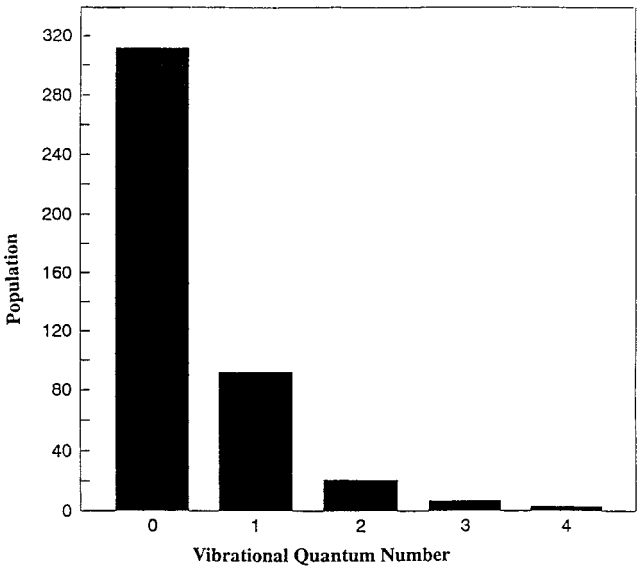

Figure 10. Vibrational population distribution of MgH at the collision energy of 2.026 kcal/mol.

anticipated to be long-lived. However, the consequences in Figures 7 and 8 indicate that the lifetime of the linear collision complex is somewhat shorter than its rotational period ($\sim 10^{-12}$ s).

The formation of a long-lived complex depends not only on the presence of potential well along the reaction coordinate but also on the nature of reactants and the translational collision energy.[27] In general, the lifetime of the complex becomes shortened with increase of the translational collision energy, and may be prolonged with increase of the reactant complexity. In this work, the forward scattering reaction is enhanced with increasing the collision energy to 8.104 kcal/mol (Figure 11b). The incoming Mg atom with higher relative velocity makes the collision complex short lived and further forces the resulting MgH product to continue forward in the center-of-mass framework. However, the increased collision energy is still less than the activation energy of 31−39 kcal/mol along a collinear approach.[14] The difference in distribution is not caused by the involvement of the collinear H-abstraction mechanism, which usually shifts the scattering distribution toward the backward direction.[26,27]

E. Rotational Population Distributions for $O(^1D) + H_2$ vs $Mg(^1P_1) + H_2$. The reaction of $O(^1D) + H_2$ has been widely investigated as a prototype for the insertion mechanism.[25,32−36] The title reaction, $Mg(3^1P_1) + H_2$, exhibits several dynamical features similar to the $O(^1D) + H_2$ reaction.[33] For instance, the reaction cross sections for both systems decrease with the kinetic energy. The scattering distributions are nearly forward−backward symmetric. The vibrational populations peak at $v = 0$ and tend to decrease with the vibrational states. Both reaction pathways are dominated by an insertion mechanism but suffer from an energy barrier for the collinear approach. Recent studies, however, revealed that when the kinetic energy exceeded ~2 kcal/mol for $O(^1D) + H_2$, the insertion mechanism may be accompanied by the abstraction pathway, and the reaction cross section increased gradually with the kinetic energy.[35,36] For both reactions, the insertive approach follows an attractive potential surface forming a short-lived collision complex such that the energy randomization is incomplete before decomposition. The $O(^1D) + H_2$ collision lies adiabatically along a single surface, and the resulting rotational distribution is single-peaked and hotter than the statistical result. Nevertheless, the title reaction

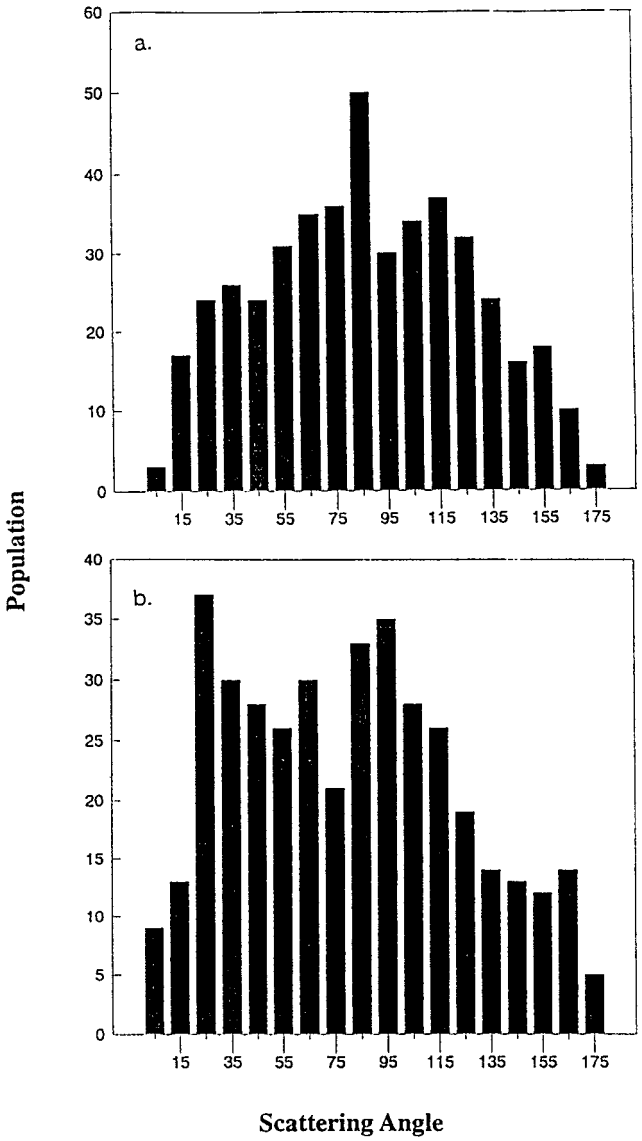

Figure 11. Angular distribution of MgH in the center-of-mass framework at the collision energies of (a) 2.026 and (b) 8.104 kcal/mol.

involves two potential surfaces and leads to a bimodal rotational distribution. For $O(^1D) + H_2$, the OH rotational distribution may be successfully interpreted by invoking an impulse collision model.[33,35] In view of the above dynamical similarities between these two systems, it is worthwhile to examine applicability of the model to the $Mg(3^1P_1) + H_2$ reaction.

For $O(^1D) + H_2$, the obtained rotational distribution may be understood as a result of hard collision between two H atoms of H_2O complex.[33] The impulse from this collision leads to equal momenta in the two atoms, and the magnitude of each momentum is determined by the energy available to the products ΔE, which denotes the energy in excess of the product vibrational energy. Accordingly, the rotational energy of the diatomic molecule can be expressed by the formula $E_{rot} = J^2/2\mu'' R_e^2$ or $[\mu'/(\mu' + \mu'')]\Delta E$.[33] Here, J is the diatomic molecule angular momentum, R_e the equilibrium distance, μ'' the diatomic reduced mass, and μ' the product translational reduced mass. According to this impulse model, Fitzcharles and Schatz found an agreement with the results of QCT calculations for the product rotational energies at different vibrational states ($v = 0$, 1, and 2) in the cases of $O(^1D) + H_2$ and $O(^1D) + D_2$. For

$O(^1D) + HD$ and $O(^1D) + DH$, the agreement is however less quantitative.[33]

As shown in Figures 4 and 5, the rotational distributions of MgH $v = 0$ and $v = 1$ give rise to the average J values of 28.9 and 25.1, respectively. The rotational energies correspond to 13.8 and 10.5 kcal/mol. If the hard collision between two H atoms dominates the MgH_2 complex dissociation, then the rotational energy difference between MgH $v = 0$ and $v = 1$ is estimated to be 2.14 kcal/mol, given the vibrational constant of 1495.20 cm^{-1}.[31] The result is in good agreement with 3.3 kcal/mol predicted by the QCT calculation. However, when the isotope effect is inspected, the model expects that the MgH product rotational energy from H_2 is smaller than that from HD.[33] The prediction is contrary to the observation in which the isotope effect was not found.[8] The hard collision model seems to be too simple to interpret satisfactorily the current reaction. In fact, in our case, the crossing seam between two potential surfaces may constrain the geometries of collision complex for an effective reaction. One may find that the H−H bond becomes dissociative when the $Mg-H_2$ reaches the crossing region.[14] The $Mg-H_2$ interaction potential may well be reduced to only one term of a diatomic potential associated with Mg and the departing H atom, while the other H remains as a spectator. Therefore, if the hard collision is applicable, the impulsive repulsion should act on Mg and the departing H atom rather than the two H atoms as in the case of $O(^1D) + H_2$.

IV. Conclusion

The quasiclassical trajectory calculations for the reaction of $Mg(3^1P_1)$ with H_2 have been performed on the excited state $^1A'$ (or $^1B_2$ in the C_{2v} symmetry) as the entrance channel and on the ground state $^1A'$ (or $^1A_1$) as the exit channel. The transition probability is considered as unity, once the trajectories go through the region of surface crossing and change to the lower surface. In this work, we have provided quantitatively several dynamical parameters for the current reaction. First, the total collisional deactivation and reaction cross sections have been calculated to decrease with increasing the collision energy. Second, the obtained rotational product distribution is characterized by a bimodal feature for both MgH $v = 0$ and 1. The high rotational distribution may be caused by a strong anisotropy of the exit channel PES, while the low rotational distribution is subject to a weak PES anisotropy. For the formation of the low-N component, elongation along the Mg−H stretching direction is not the only pathway. Third, in the calculation of the angular product distribution, a near symmetry with respect to the scattered angle at 90° indicates that the reaction proceeds predominantly via a linear collision complex. Increasing the collision energy may shift the distribution toward a forward direction. Finally, the vibrational product distribution is calculated to decrease with the quantum numbers, in agreement with the experimental findings. Nevertheless, the resulting ratio of MgH(v=1) to MgH(v=0) is underestimated. The discrepancy might arise from the shortcomings involved in the initial conditions and the incomplete energy redistribution in the exit channel.

Acknowledgment. The authors wish to thank Professors F. E. Budenholzer and J. M. Yuan for helping with the QCT program and useful discussion. They also thank professors D. Gerlich and P. D. Kleiber for critical reading of the manuscript and providing valuable comments. This work is supported by the National Science Council of the Republic of China under the Contract NSC87-2113-M-001-021 and NSC88-2113-M-002-011.

References and Notes

(1) Bililign, S.; Kleiber, P. D. *J. Chem. Phys.* **1992**, *96*, 213.
(2) Bililign, S.; Kleiber, P. D.; Kearney, W. R.; Sando, K. M. *J. Chem. Phys.* **1992**, *96*, 218.
(3) Neumark, D. M.; Wodke, A. M.; Robinson, G. N.; Hayden, C. C.; Lee, Y. T. *J. Chem. Phys.* **1985**, *82*, 3045.
(4) Polanyi, J. C.; Schreiber, J. L.; Sloan, J. J. *Chem. Phys.* **1975**, *9*, 403.
(5) Liu, D. K.; Lin, K. C. *J. Chem. Phys.* **1996**, *105*, 9121.
(6) Liu, D. K.; Lin, K. C. *J. Chem. Phys.* **1997**, *107*, 4244.
(7) Breckenridge, W. H.; Umemoto, H. *J. Chem. Phys.* **1984**, *80*, 4168.
(8) Breckenridge, W. H.; Wang, J. H. *Chem. Phys. Lett.* **1987**, *137*, 195.
(9) Kleiber, P. D.; Lyyra, A. M.; Sando, K. M.; Zafiropulos, S. V.; Stwalley, W. C. *J. Chem. Phys.* **1986**, *85*, 5493.
(10) Kleiber, P. D.; Lyyra, A. M.; Sando, K. M.; Heneghan, S. P.; Stwalley, W. C. *Phys. Rev. Lett.* **1985**, *54*, 2003.
(11) Chaquin, P.; Sevin, A.; Yu, H. *J. Phys. Chem.* **1985**, *89*, 2813.
(12) Lin, K. C.; Huang, C. T. *J. Chem. Phys.* **1989**, *91*, 5387.
(13) Liu, D. K.; Chin, T. L.; Lin, K. C. *Phys. Rev. A* **1994**, *50*, 4891.
(14) Ou, Y. R.; Liu, D. K.; Lin, K. C. *J. Chem. Phys.* **1998**, *108*, 1475.
(15) Blickensderfer, R. P.; Jordan, K. D.; Adams, N.; Breckenridge, W. H. *J. Chem. Phys.* **1982**, *86*, 1930.
(16) Schinke, R. *Photodissociation Dynamics*; Cambridge University Press: Cambridge, 1993.
(17) Andresen, P.; Schinke, R. In *Molecular Photodissociation Dynamics*; Ashfold, M. N. R., Baggott, J. E., Eds.; Royal Society of Chemistry: London, 1987.
(18) Sorbie, K. S.; Murrell, J. N. *Mol. Phys.* **1975**, *29*, 1387.
(19) Murrell, J. N.; Carter, S.; Farantos, S. C.; Huxley, P.; Varandas, A. J. C. *Molecular Potential Energy Functions*; John Wiley & Sons: New York, 1984.
(20) Dunham, J. L. *Phys. Rev.* **1932**, *41*, 721.
(21) Chapman, S.; Bunker, D. L.; Gelb, A. *QCPE* **1974**, *273*.
(22) Truhlar, D. G.; Muckerman, J. T. In *Atom-Molecule Collision Theory: A Guide for the Experimentalist*; Bernstein, R. B., Ed.; Plenum: New York, 1979.
(23) Smith, I. W. M. *Kinetics and Dynamics of Elementary Gas Reactions*; Butterworth: London, 1980; pp 89−94.
(24) Karplus, M.; Porter, R. N.; Sharm, R. D. *J. Chem. Phys.* **1965**, *43*, 3259.
(25) Schinke, R.; Lester, W. A., Jr. *J. Chem. Phys.* **1980**, *72*, 3754.
(26) Gilibert, M.; Aguilar, A.; Gonzalez, M.; Sayos, R. *J. Chem. Phys.* **1993**, *99*, 1719.
(27) Levine, R. D.; Bernstein, R. B. *Molecular Reaction Dynamics and Chemical Reactivity*; Oxford University Press: Oxford, 1987; Chapter 7.
(28) Breckenridge, W. H.; Umemoto, H. *J. Chem. Phys.* **1981**, *75*, 698.
(29) Hung, Y. M.; Sando, K. M. Unpublished work. Also, see: Hung, Y. M. Ph.D. dissertation, University of Iowa, 1997.
(30) Breckenridge, W. H.; Wang, J. H. *Chem. Phys. Lett.* **1987**, *139*, 28.
(31) Hubers, K. P.; Herzberg, G. *Constants of Diatomic molecules*; van Nostrand: Princeton, 1979.
(32) Butler, J. E.; Jursich, G. M.; Watson, I. A.; Wiesenfeld, J. R. *J. Chem. Phys.* **1986**, *84*, 5365.
(33) Fitzcharles, M. S.; Schatz, G. C. *J. Phys. Chem.* **1986**, *90*, 3634 and references therein.
(34) Kuntz, P. J.; Niefer, B. I.; Sloan, J. J. *J. Chem. Phys.* **1991**, *151*, 77.
(35) Schatz, G. C.; Papaioannou, A.; Pederson, L. A.; Harding, L. B.; Hollebeck, T.; Ho, T. S.; Rabitz, H. *J. Chem. Phys.* **1997**, *107*, 2340.
(36) Hsu, Y. T.; Wang, J. H.; Liu, K. *J. Chem. Phys.* **1997**, *107*, 2351 and references therein.